Proceedings

Development of Yttrium-Cerium oxide gas sensor for low ppm Hydrogen detection[†]

Shivangi Srivastava[1]*, N.K. Pandy[1], V. Verma[1], P. Singh[1], A. Verma[1], N. Yadav[1], P.K. Pandey[2], J. Sarkar[2]

[1] Department of Physics, University of Lucknow, Lucknow 226007, India; profnaredrapandey137@gmail.com
[2] Department of Chemistry, University of Lucknow, Lucknow 226007, India; dr.joysarkar4@gmail.com
* Correspondence: shivangsrivastav007@gmail.com
† Presented at **The 4th International Electronic Conference on Applied Sciences, (ASEC 2023), 27 October– 10 November 2023; Available online: https://asec2023.sciforum.net**

Abstract: The hydrothermal method was successfully used in the current work to fabricate YCeO nanocomposites, a novel hydrogen (H_2) gas sensor. XRD, FE-SEM, AFM were performed for knowing the crystal structure and morphology of as prepared nanocomposite. The cubic structure of space group Fm3m with a density of 6.74 $gmcm^{-3}$, a volume of 157.81 10^6 pm^3, and a crystallite size of 18.66 nm is gotten in the XRD pattern of YCeO in this instance. Furthermore, the granular structure and roughness of the surface can be seen in FE-SEM and AFM studies. Additionally, Hydrogen sensing was performed at temperature of 28°C with hydrogen concentration of 20-120 ppm. The sensor response for hydrogen gas at 20 and 120 ppm was measured to be 1.41 and 2.09, respectively. At 20 ppm, came to know that the recovery times and rapid response were 75.54 s, and 40.81 s respectively. The long-time stability was also checked for 40 days and got the change in sensor response at 20 and 40 days was 1.40 and 1.39 receptively. The investigated sensor device also demonstrates the benefits of a straightforward fabrication procedure, a basic structure, and a very affordable hydrogen detection sensor.

Keywords: Cerium oxide; Yttrium oxide; Nanocomposite; Morphology, H_2 Gas Sensing; Mechanism

1. Introduction

For energy storage and extraction in different manufacturing unit, including different industries, transportation, and domestic consumption, hydrogen gas (H_2) is essential. However, H_2 is hazardous to handle and use at high temperatures since it is combustible, odorless, and colorless [1,2]. It is being considered to use H_2 gas as a potential substance for use in a variety of fields, such as aeronautical engineering, power production, chemical goods, transportation, and medical biomarkers. However, it is invisible to human senses and traditional gas sensors due to issues including high permeability, flammability, intense chemical reactivity, and absence of odor, taste, and color. It is crucial to detect H_2 gas molecules at normal temperature. Devices based on semiconducting metal oxide are dependable and long-lasting for H_2 gas detection. Metal oxides consisting of tungsten, tin, molybdenum, niobium, and zinc have been found to be reliable and fast at detecting H_2 gas [3–6]. In general, all these applications call for specified properties in nanoparticles. The nanoparticles made from cerium oxide have produced significant advances in biological sciences, industry, and other fields; besides having all these uses been found to be essential for humanity, considerably aiding in the worldwide growth of number of industries. However, yttrium oxide nanoparticles have a variety of uses for the study of materials. A key building block for an inorganic synthesis of compounds, yttrium oxide has the capacity to generate the red color, which is a characteristic employed in fluorescent illumination. The exploration of innovative CeO_2/Y_2O_3 composites with tiny pores and a

structure that is cubic, that are attractive candidates for a range of uses because of enormous area of the surface, low noxiousness and stability, is, however, the subject of fewer research papers now [7–11]. As a result, we described fabrication and characteristics of CeO_2/Y_2O_3 nanocomposites produced by the hydrothermal process, a straightforward method to produce nanostructures using water as solvent at extreme vapor pressures and low temperatures in an autoclave coated in Teflon. Following that FE-SEM, XRD, and AFM were used to further understand the structural and morphological characteristics of the as-prepared materials. Lastly, Hydrogen sensing was performed at low ppm.

2. Materials and Synthesis

High-purity chemical reagents of srl grade were then employed in the current work without additional purification. For the creation of the combination of nanoparticles, we employ hydrothermal synthesis. Enough 0.1M Cerium (III) nitrate hexahydrate and 0.1M Yttrium (III) nitrate hexahydrate were dissolved for six hours in distilled water to maintain the homogenous solution. In parallel, distilled water was used to completely dissolve 0.5M of NaOH. At the ambient temperature, NaOH was then progressively added drop by drop until the pH was 10–11. After that, the whole solution was heated for a period of eight hours at 160°C in a 100ml Teflon-lined autoclave. The autoclave was then carried out and permit to cool at ambient temperature; this produced a small amount of Precipitate that is light yellow, which was then dried in a 100°C oven. In order to create powdered nanocomposite YCeO, 550 °C was used for annealing the material, and after that it was given time to cool to room temperature. This mixture was then combined with the cerium/yttrium nanocomposites.

2.1. Device Fabrication and Measurement Setup

The YCeO sensing film was untrue on a glass substrate1 by using spin coating method. The glass substrate (dimension 1×1 cm^2) was cleaned resulting with distilled water and acetone instead by ultrasonication. Then substrate was dry at 60°C for 20 mins to eliminate organic rests. On the other hand, YCeO powder was discrete in dimethyl formamide (DMF) and standardized solution was found. Now the homogenous solution was dropped on glass substrate and spin coat at 1500 rpm for 50 s and then dry on a hot plate for 20 min at 50°C. This process was repeated for 2 times to get the obligatory thickness and lastly the thin film was annealed at 400°C for 2 h in furnace. After that, silver electrodes were dropped on sensing film. This sensing device was positioned inside the sensing setup and connected to end of Keithley electrometer. All the gasses used in measurement by gas cylinders.

3. Results and Discission

Using powder X-ray diffraction (PXRD), a non-destructive analytical technique for differentiating the different crystal-line phases of binary metal oxide nanocomposite, the crystalline phase of the fabricated materials was evaluated. The X-ray diffraction pattern's recorded peaks were all found to be phases of either yttrium oxide or cerium oxide, and all the diffraction peaks are perfectly coincident with the binary metal oxide's cubic phase. It also exhibits the excellent crystallinity of the fabricated NPs and their independent cubic fluorite phase in the (Fm3m) space group. To determine the crystal and phase structure of the Yttrium Cerium oxide, PXRD was used; the resulting x-ray pattern is given in Fig. 1. (a), The (420), (331), (400), (222), (311), (220), (200), and (111) miller indices correlate to the cubic structure of YCeO, and distinct 2θ peaks were found at 79.207, 76.827, 69.524, 59.179, 56.427, 47.553, 33.128, and 28.587.[12].

The NPs' quality and shape were fundamental elements when examining interactions between nanomaterials. Here, FE-SEM was used to analyses the morphological analyses was shown in Fig.1. (b). Under various magnifications, the FE-SEM micrograph was acquired to examine the diameter ranging from 10 to 50 nm of the granular form. The

combination of yttrium and cerium to form a nanocomposite structure may be observed clearly in the image, or we can say that both nanoparticles typically exhibit the same shape as fused and aggregated nanoparticles. These granular structures have both a porous shape and an impressive, endless surface area. By analyzing these nanocomposites, we may conclude that it is a precise and economical method of synthesizing YCeO. These tiny YCeO granules increase the material's area of the surface and porosity, that is particularly valuable for the adsorption of analytes and enhances the performance of gas sensing.

AFM analysis is the best technique for statistically determining the nanometric dimensional surface roughness and for showcasing the surface nanotexture of the deposited film as shown in Fig.1. (c). Like what was seen in the SEM investigation, the surface of the as-grown YCeO films has a granular texture. However, In the AFM images, the crystallites seem larger due to tip convolution. The SEM images demonstrate that the boundaries of the microscopic splits between the grains appear less sharp for a similar reason. In contrast to the "hill" area, it has several orientation-specific crystal-like structures, the "valley" zone is rather smooth. Mean roughness was 40.34 nm, while RMS roughness was 52 nm, and average roughness was 130.94 nm according to the estimated value.
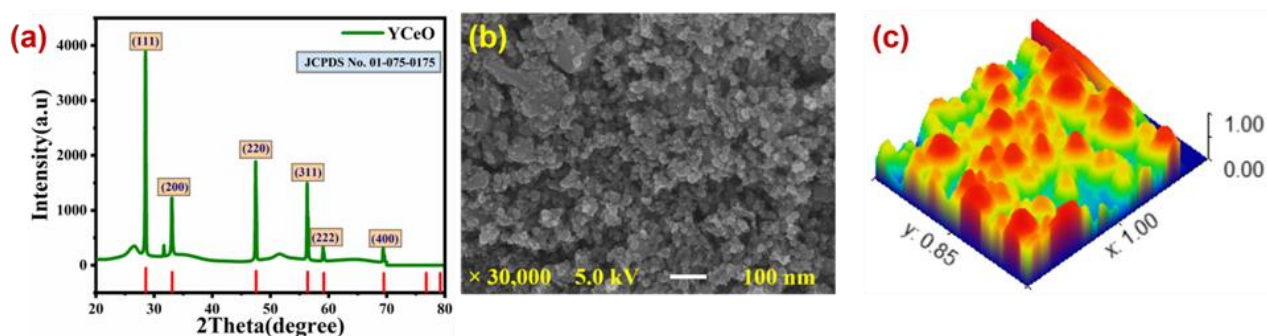

Figure.1. (a) shows the XRD spectrum, (b) shows the FE-SEM micrograph on 100 nm and (c) shows the AFM micrograph of as-prepared YCeO.

4. H_2 Gas Sensing

The response of the fabricated sensor based on YCeO were tested at the range of 20-120 ppm H_2 gas is shown in Fig. 2(a). Here, we detected an even graph with less variations which is suggesting that the response enhancing was due to YCeO based sensor. The response to H_2 at 28°C reached its maximum peak thus, this was suggesting that the finest operating temperature is 28°C should be chosen.

According to the sensor response vs. concentration linear fitting curve, as seen in Fig. 2(b), the sensor response representation about linearly as concentration increased. The linearity coefficient (R^2) was determined to be 0.99, indicating the accuracy of a curve that fits linearly. The lowest and highest sensor response values for YCeO were determined to be 1.41 and 2.09, respectively. The YCeO sensor's sensitivity is additionally determined by the slope of the curve between the constant sensor response and concentration. In the region of 20 to 120 ppm, it was discovered that the YCeO sensor's sensitivity was 0.067 sensor response/ppm.

$$S = \frac{I_g}{I_a} \qquad (1)$$

$$S = A[C]^n + B \qquad (2)$$

Where [C] stands for analyte gas concentration and A & B are both constants. Both response and recovery time for YCeO based sensor are protracted with the increase of H_2

concentration. The recovery time is the amount of time needed to lessen the gap between the maximum and lowest current, and the response time (tres) is the amount of time required for the relative current change to reach 90% of the steady state value following H_2 injection[13–16] . As shown in Fig. 2(c) and (d) the YCeO sensor demonstrated a decent response at 28°C and almost linear growth with H_2 concentrations. Further research on the YCeO-based sensor to 20–120 ppm H_2 at 28°C revealed that the current decreased following injection into 20 ppm H_2 and returned to its previous value upon discharge of H_2 vapors. The results showed that 40.81 seconds and 75.54 seconds, respectively, were the lowest response and recovery times. The current of the sensor film likewise increased as concentration grew. Lower H_2 concentrations result in a weaker connection between H_2 molecules and adsorbed oxygen species, whereas higher H_2 concentrations signify a rise in the sensing film's current. The slope of the linear fitting curve of sensor response vs. concentrations is used to determine sensitivity. The response and recovery times of YCeO based sensor for every concentration were estimated by following Eqn. (3-4).

$$I(t) = I_a \left(e^{\frac{t}{t_{res}}} \right) \quad (3)$$

$$I(t) = I_a \left(1 - e^{-\frac{t}{t_{res}}} \right) (4)$$

This recommends that the gas sensor created on the YCeO can comprehend faster detection of H_2 vapor at low concentration. The high sensor response and rapid response-recovery abilities of a sensor must be recurring by functioning use of the large surface area and surface approachability.

Based on the findings of the experiments, the limit of detection (LOD) for the YCeO-based chemo resistive gas sensor was determined by Eqn. (5)

$$LOD = \frac{3.3 \times \sigma}{m} \quad (5)$$

Here, m is slope of linear fit curve and σ is standard deviation of intercept. The LOD of YCeO-based chemo resistive gas sensor was found to be 13.24 ppm.
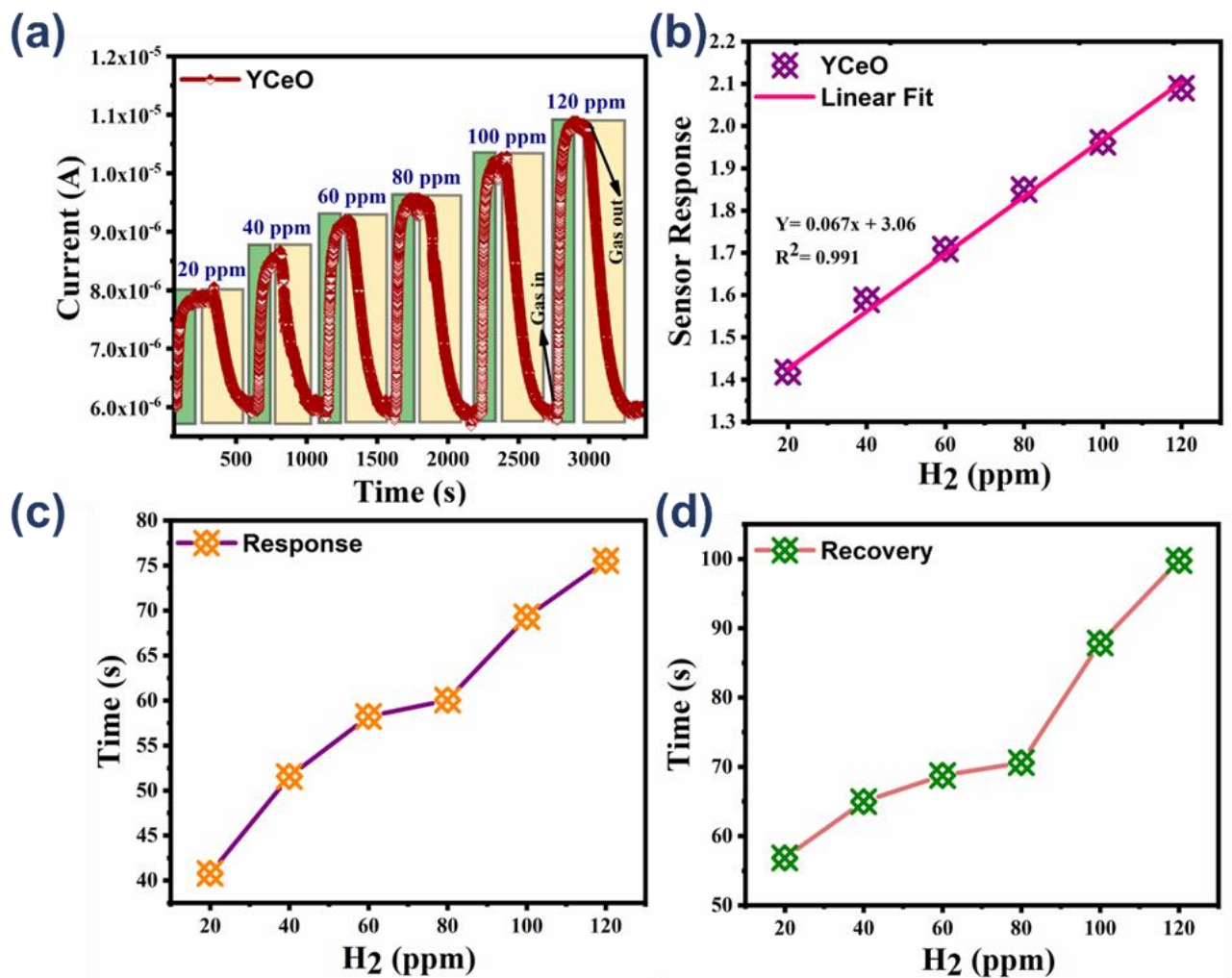
Figure.2. (a) Sensing characteristics curve of YCeO nanorod at different concentration (20-120 ppm), (b) and (c) response and recovery time graph (d) Sensor response linear fit graph.

Here Fig.3. (a) shows the great repeatability of 6 cycles at 20 ppm of H_2 which shows the excellent repeatability. Sensor selectivity is the ability of a sensor to detect a particular gas in the presence of other gases. In other words, by likening the effects of various gases (oxidizing or reducing) on the sensor response, the selectivity may be calculated. Fig. 3. (b) depict the YCeO gas selectivity towards several gases at room temperature, including NH_3, H_2S, NO_2, and H_2. Furthermore, the detected current of NH_3, H_2S and NO_2 were low and unstable in comparison to the H_2 gas current. In the presence of NH_3, H_2S and NO_2 gases, it seems that YCeO thin film has the best selectivity towards H_2, which confirms that H_2 gas molecules are more adsorbent on the surface of YCeO than NH_3, H_2S and NO_2 gases, as seen in Fig. 3. (b). For sensor optimizations, long-term stability and repeatability of the sensor are critical partners. A gas sensor's feature life is also essential to its economic development. By measuring the reactions of the YCeO sensor to 20 ppm H_2 at room temperature (28 °C) for 40 days, the sensor's long-term dependability was investigated as shown in Fig.3. (c). The sensor showed extremely little current and response value changes, indicating strong long-term reliability. The sensor indicates that, after 20 and 40 days, the rapid sensor response was 1.40 and 1.39, respectively as shown in Fig.3. (d). This result indicates that physisorption, as contrasting to chemisorption, dominates the

interactivity between surface of the as-prepared sample and H_2 gas. This long-term stability provides additional support for its likely industrial uses.
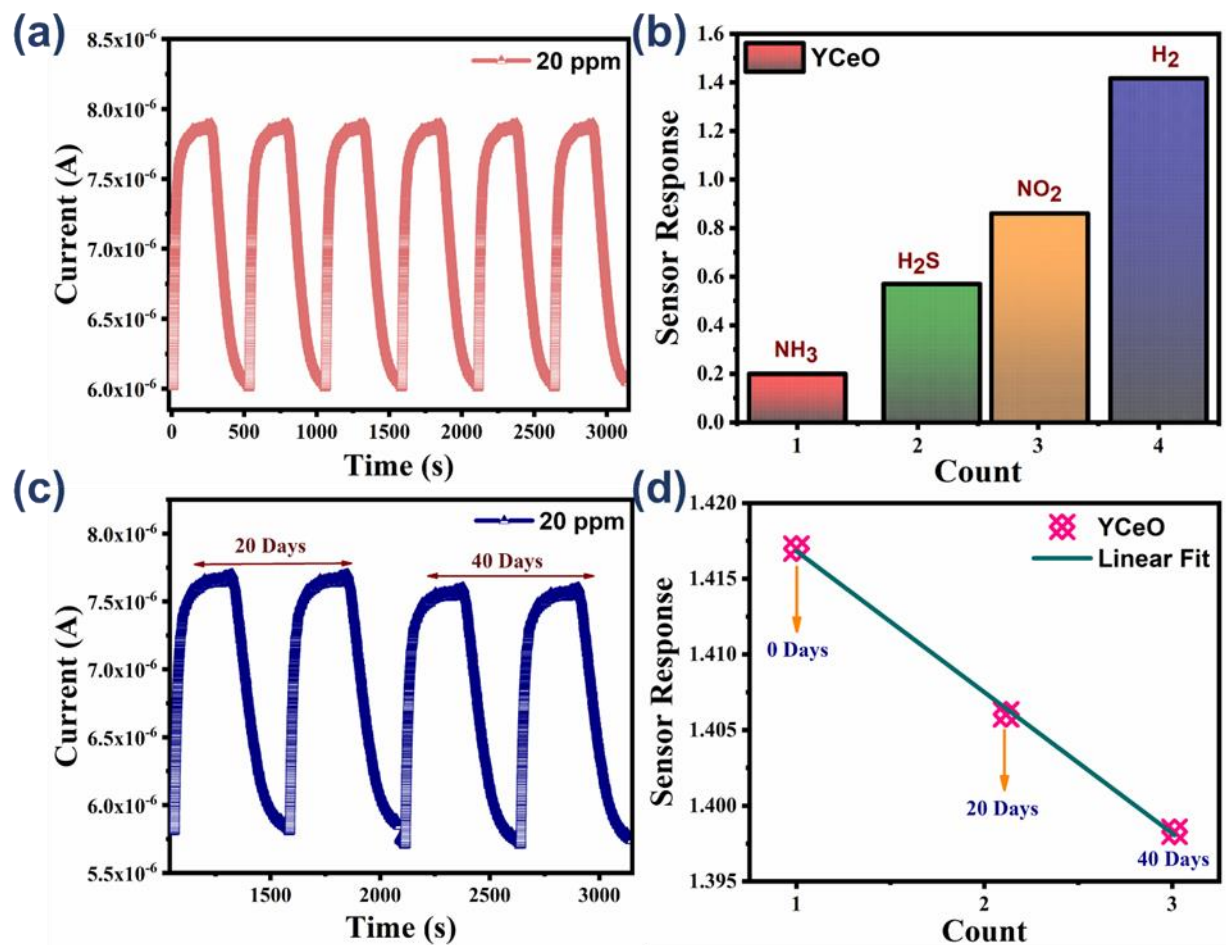

Figure.3. (a) shows the repeatability at 20 ppm, (b) shows the selectivity curve of YCeO sensor towards exposure of numerous gases, (c) shows the durability curve for 40 days towards at 20 ppm exposure of H_2, and (d) Sensor response curve for 40 days.

The conventional metal oxide semiconductor gas sensors' detecting mechanism, particularly hydrogen gas sensing by YCeO-based sensors, is discussed. The current modulation of the YCeO layer is influenced by the chemisorption of oxygen molecules and atoms on the YCeO surface. This results in a negative surface charge, forming a depleted region under the surface. In the nanocrystalline layer. The surface of the YCeO semiconductor can easily absorb oxygen in air, forming chemisorbed oxygen ions O_2^- or O^-.

When hydrogen is introduced, the surface charged decreases due to the reaction of chemisorbed O_2 species with H_2, resulting in increased sensor current. When loaded with target gas, the sensor chamber reacts containing oxygen ions that have been adsorbed, reducing the depletion region width and allowing trapped electrons to move back to the conduction region. For hydrogen, the highest sensor response is shown at even ppm values with the greatest shift in the depletion region. The responsiveness of the sensor is also affected by its operational temperature and targeted concentration of gas. As temperature rises, oxygen ions are more readily chemisorbed, leading to a large change in depletion region and sensor resistance. With increasing gas concentration, the sensor responsiveness is further improved by a significant interaction with adsorbed oxygen ions. [17,18].

Furthermore, this suggests that the gas sensor based on the YCeO-based chemo resistive gas sensor can realize faster detection of H_2 at low concentration. The high response and quick response-recovery abilities of a sensor must be sustained by effective use of the

large surface area and surface approachability. In comparison to previously reported work, YCeO-based chemo resistive gas sensor showed high sensing performance at room temperature as mentioned in Table 1.

Table.1. Comparative study of H_2 Sensors.

Material	Temp. (°C)	Conc. (ppm)	Response time (s)	Recovery Time (s)	Ref.
SnO_2	130	5000	2	10	[19]
In_2O_3	260	500	1.7	1.5	[20]
Pd-ZnO nanowires	250	100	25	52	[21]
Pd/In_2O_3	225	0.1	12	-	[22]
YCeO	28	20	1.41	2.09	Present Work

Moreover, we suggest that the semiconductor YCeO plays a role of catalyst for the interaction between H_2 and atomic oxygen. These outcomes indicate that the reported H_2 sensors based on YCeO that were prepared at low temperature can be operative to achieve superior sensing performance equated to their counterparts.

Conclusion

At room temperature (28°C), the results of a YCeO-based chemo resistive gas sensor for the detection of H_2 were excellent. XRD research was done to determine the YCeO nano-composite's structural details. Furthermore, FE-SEM and AFM was performed to know the morphology of as prepared material. H_2 was revealed at ambient temperature in the range of 20-120 ppm. At 20 or 120 ppm, the sensor response for H_2 was determined to be 1.41 and 2.09, respectively. At 20 ppm, it was found that the rapid response and recovery times were 40.81 s and 75.54 s, respectively. The long-time stability was also checked for 40 days and got the change in sensor response at 20 and 40 days was 1.40 and 1.39 receptively. The successful creation of a nanocomposite between Y_2O_3 and CeO_2 was the cause of the improved sensor response, which led to improved sensing performance. The chemo resistive gas sensor built on YCeO successfully demonstrated great long-term stability, exceptional sensor responsiveness, quick response/recovery, and selectivity to H_2 in comparison to other gases. This study reveals the YCeO chemo resistive sensor's exceptional potential as a low-trace H_2 gas detector.

References

1. Ou JZ, Yaacob MH, Campbell JL, Breedon M, Kalantar-Zadeh K, Wlodarski W. H2 sensing performance of optical fiber coated with nano-platelet WO3 film. Sens Actuators B Chem. 2012;166–167:1–6.

2. Yaacob MH, Ahmad MZ, Sadek AZ, Ou JZ, Campbell J, Kalantar-Zadeh K, et al. Optical response of WO3 nanostructured thin films sputtered on different transparent substrates towards hydrogen of low concentration. Sens Actuators B Chem. 2013; 177:981–8.

3. Partridge JG, Field MR, Peng JL, Sadek AZ, Kalantar-Zadeh K, Du Plessis J, et al. Nanostructured SnO $_2$ films prepared from evaporated Sn and their application as gas sensors. Nanotechnology. 2008; 19:125504.

4. Rahmani MB, Keshmiri SH, Yu J, Sadek AZ, Al-Mashat L, Moafi A, et al. Gas sensing properties of thermally evaporated lamellar MoO3. Sens Actuators B Chem. 2010; 145:13–9.

5. Sadek AZ, Choopun S, Wlodarski W, Ippolito SJ, Kalantar-Zadeh K. Characterization of ZnO Nanobelt-Based Gas Sensor for ${\rm H} _{2}$, ${\rm NO}_{2}$, and Hydrocarbon Sensing. IEEE Sens J. 2007; 7:919–24.

6. Barrak H, Saied T, Chevallier P, Laroche G, M'nif A, Hamzaoui AH. Synthesis, characterization, and functionalization of ZnO nanoparticles by N-(trimethoxysilylpropyl) ethylenediamine triacetic acid (TMSEDTA): Investigation of the interactions between Phloroglucinol and ZnO@TMSEDTA. Arabian Journal of Chemistry. 2019; 12:4340–7.

7. Balĺee E, Ringuedé A, Cassir M, Putkonen M, Niinistö L. Synthesis of a thin-layered ionic conductor, CeO2-Y2O3, by atomic layer deposition in view of solid oxide fuel cell applications. Chemistry of Materials. 2009; 21:4614–9.

8. Tadokoro SK, Morcillo ENS. Influence of the precursor purity and the precipitating agent on impedance spectroscopy of CeO2:Y2O3 ceramics. J Alloys Compd. 2004. p. 190–3.

9. Kaviyarasu K, Manikandan E, Nuru ZY, Maaza M. Investigation on the structural properties of CeO2 nanofibers via CTAB surfactant. Mater Lett. 2015; 160:61–3.

10. Berutti FA, Alves AK, Bergmann CP, Clemens FJ, Graule T. Synthesis of CeO2 and Y2O3-Doped CeO2 composite fibers by electrospinning. Particulate Science and Technology. 2009; 27:203–9.

11. Magdalane CM, Kaviyarasu K, Vijaya JJ, Siddhardha B, Jeyaraj B, Kennedy J, et al. Evaluation on the hetrostructured CeO2/Y2O3 binary metal oxide nanocomposites for UV/Vis light induced photocatalytic degradation of Rhodamine - B dye for textile engineering application. J Alloys Compd. 2017; 727:1324–37.

12. Srivastava S, Pandey NK. Low-Cost Hydrothermally Synthesized Multifunctional Rare Earth Metal Yttrium Cerium Oxide. IOCN 2023. Basel Switzerland: MDPI; 2023. p. 26.

13. Verma V, Pandey NK, Gupta P, Singh K, Singh P. Humidity sensing enhancement and structural evolution of tungsten doped ZnO nanosensors fabricated through co-precipitation synthesis. Physica B Condens Matter. 2021; 619:413224.

14. Singh P, Pandey NK, Awasthi RR, Siva Kumar VV, Verma V, Kumar B, et al. Analysis of the optical, chemical, surface, and humidity sensing characteristics of nanostructured Bi2O3-doped MoO3 materials. Mater Today Proc. 2023;

15. Singh A, Singh A, Verma A, Yadav BC, Chaudhary V. Economic ZnCo2O $_4$ Nanoflakes Chemiresistor Assisted Room-Temperature Monitoring of Low Trace Airborne Ammonia. ECS Journal of Solid-state Science and Technology. 2023; 12:047005.

16. Singh A, Yadav SK, Verma A, Sikarwar S, Yadav BC. Hydrothermally Synthesized ZnSnO $_3$ Nanoflakes Based Low-Cost Sensing Device for High Performance CO $_2$ Monitoring. ECS Advances. 2023; 2:016501.

17. Singh A, Sikarwar S, Verma A, Chandra Yadav B. The recent development of metal oxide heterostructures based gas sensor, their future opportunities and challenges: A review. Sens Actuators A Phys. 2021; 332:113127.

18. Singh A, Sikarwar S, Yadav BC. Design and fabrication of quick responsive and highly sensitive LPG sensor using ZnO/SnO $_2$ hetrostructured film. Mater Res Express. 2021; 8:045013.

19. Adamyan, AZ (Adamyan, A. Z.) ; Adamyan, ZN (Adamyan, Z. N.). Sol-gel derived thin-film semiconductor hydrogen gas sensor. International Journal of Hydrogen Energy. 2007; 32:4101-4108.

20. Li, ZJ (Li, Zhijie) ; Yan, SN (Yan, Shengnan) Hydrogen gas sensor based on mesoporous In_2O_3 with fast response/recovery and ppb level detection limit. International Journal of Hydrogen Energy. 2018; 43:22746-22755.

21. Kwon, YM (Kwon, Yeong Min) Ce oxide nanoparticles on porous reduced graphene oxides for stable hydrogen detection in air/HMDSO environment. Sensors And Actuators B- Chemical. 2020; 321.

22. Yang, YC (Yang, Yu-Chung). Study of a Palladium Nanoparticle/Indium Oxide-Based Hydrogen Gas Sensor. IEEE Transactions on Electron Devices. 2022; 69:318-324.